NASA TECHNICAL NOTE

NASA TN D-3018

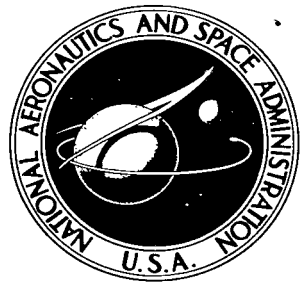

NASA TN D-3018

HYPERVELOCITY IMPACT DAMAGE CHARACTERISTICS IN BERYLLIUM AND GRAPHITE PLATES AND TUBES

by James H. Diedrich, Irvin J. Loeffler, and A. R. McMillan

NATIONAL AERONAUTICS AND SPACE ADMINISTRATION • WASHINGTON, D. C. • SEPTEMBER 1965

HYPERVELOCITY IMPACT DAMAGE CHARACTERISTICS IN BERYLLIUM AND GRAPHITE PLATES AND TUBES

By James H. Diedrich, Irvin J. Loeffler,

Lewis Research Center
Cleveland, Ohio

and A. R. McMillan

General Motors Corporation
Defense Research Laboratories
Santa Barbara, Calif.

NATIONAL AERONAUTICS AND SPACE ADMINISTRATION

For sale by the Clearinghouse for Federal Scientific and Technical Information
Springfield, Virginia 22151 – Price $2.00

HYPERVELOCITY IMPACT DAMAGE CHARACTERISTICS IN BERYLLIUM AND GRAPHITE PLATES AND TUBES

by James H. Diedrich, Irvin J. Loeffler,

Lewis Research Center

and A. R. McMillan

General Motors Corporation
Defense Research Laboratories
Santa Barbara, California

SUMMARY

Experiments were conducted on beryllium and graphite to determine their behavior under hypervelocity impact. Both materials were impacted with 1/8- and 3/32-inch-diameter spherical projectiles of pyrex and aluminum accelerated to a nominal velocity of 25 000 feet per second by an accelerated reservoir light gas gun. The targets were in the form of flat plates and tubes and were generally tested at temperatures of 70°, 700°, or 1300° F. Beryllium metal was tested as hot-pressed disks and as tubes fabricated from sintered-powder, cast, and extruded material. All beryllium tubular targets had high-strength inner liners. The various graphite compositions that were tested included flat blocks of ATJ, ZTA, and pyrolytic graphite. A tubular target of AGSR graphite was also tested. These selections reflected a range of densities for the graphite and a range of purities and processing methods for the beryllium.

Each material exhibited characteristic brittle crater damage and supplementary cracking damage. The cracking damage was influenced by target size and shape and for beryllium by the processing method of the armor material. The projectile penetration depths were correlated with a frequently used empirical penetration criterion based on target modulus of elasticity. The beryllium crater data exhibited a correlation within the range of experience for other metals while the graphite exhibited penetration depths below the values for metals. Design implications of the results for space radiator applications were discussed.

INTRODUCTION

Future space missions will require large amounts of electric power to satisfy main propulsion and auxiliary power requirements (ref. 1). The major requirements posed for these power-generating systems are low specific weight (lb/kW), long life (10 000 hr

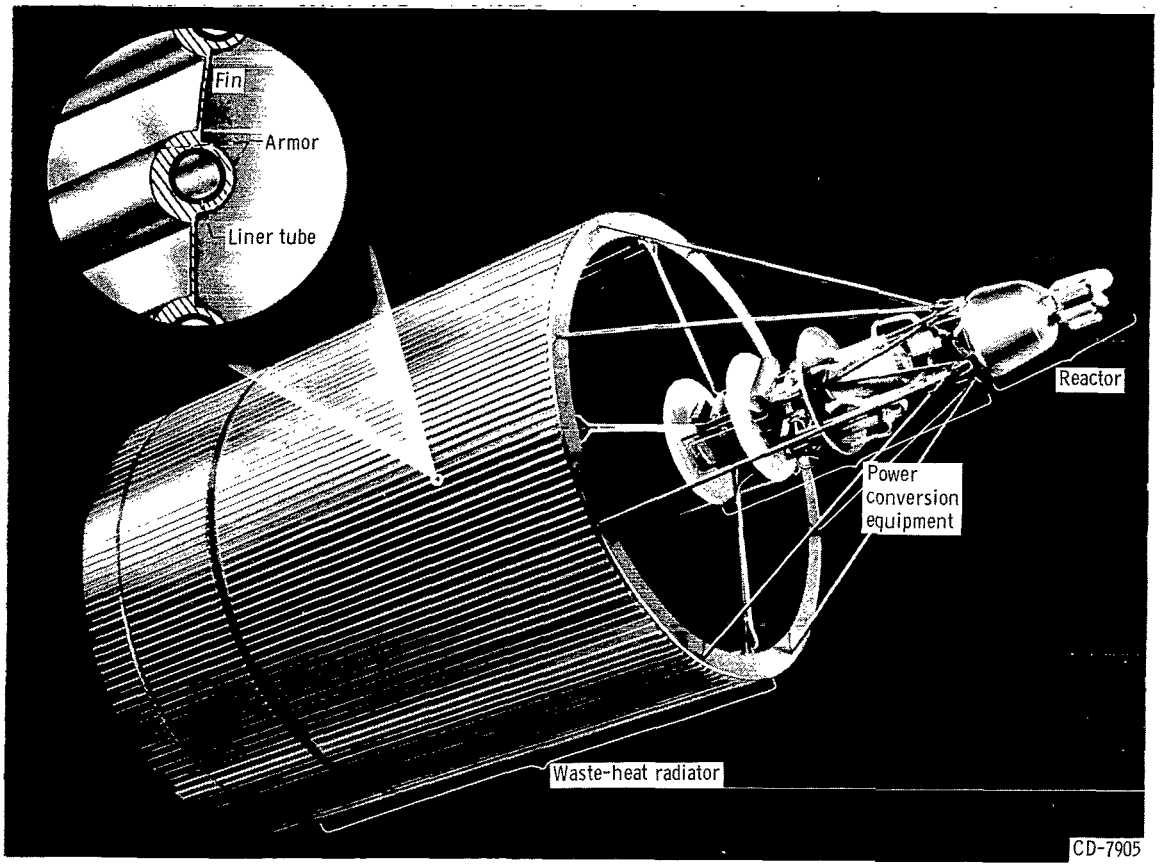

Figure 1. - Nuclear-electric space power generating system.

or more), and continuous and reliable operation. Analyses of such systems (e. g., ref. 2) have indicated that the waste-heat radiator is a major contributor to the total powerplant weight and that the majority of this weight is concentrated in the protective armor on the radiator surfaces vulnerable to damage by impacting meteoroids. In general, the armor is used as a sleeve or block around the fluid-carrying tube liner. A concept of a waste-heat radiator is shown in figure 1. The inset is included to show the protective armor.

The material used for the armor structure has a marked effect on the overall powerplant weight. An analysis of the effect of construction materials on total radiator weight was made in reference 3 for a system with a high power level. The armor materials that produced the lowest weight radiator for a 1-megawatt-output Rankine system with a radiator temperature of 1200° to 1400° F were beryllium and graphite. The use of more conventional materials, such as stainless steel and columbium alloy, resulted in considerably heavier radiators. Radiators with beryllium and graphite as armor were also shown in reference 3 to be potentially lighter than aluminum radiators. Therefore, there is an incentive to consider the use of beryllium and graphite for radiator armor when striving for low specific weight powerplants.

The calculated relative weight advantage of beryllium and graphite was based on their thermal conductivity, density, and hypothetical ability to resist penetration by impacting projectiles; however, the true behavior of these materials under impact is for the most part unknown. Therefore, it was necessary to investigate the impact resistance of these materials under hypervelocity impact conditions before any further assessment could be made of their potential suitability as radiator construction materials.

Materials subjected to hypervelocity impact exhibit two distinct modes of damage: primary damage due to the direct action of the projectile on the target, and secondary damage due to the interactions between the impact-generated stress waves and target boundaries (ref. 4). Brittle materials have characteristic primary and secondary damage that differs from the more ductile engineering materials. Secondary damage in brittle materials is influenced by changes in specimen size, shape, and materials in contact with the free surface (ref. 5). Furthermore, brittle materials generally exhibit greater total area damage because they are more sensitive than ductile materials to secondary damage effects. The evaluation of beryllium and graphite under hypervelocity impact conditions was undertaken to determine the primary and secondary damage characteristics for configurations applicable as meteoroid armor and to correlate the primary crater depths with an empirical penetration criterion for use in design calculations.

The approach taken in the investigation was to impact beryllium and graphite targets of commercially available compositions at room temperature and representative radiator operating temperatures with single projectiles from an accelerated-reservoir light-gas gun. The projectile mass was selected to yield impact energies typical of the energies of meteoroids that present a hazard to space radiators as stated in reference 6. Beryllium and graphite targets were fabricated in the form of flat plates and tubes by using currently available materials. All impact testing was performed under contract with the General Motors Corporation Defense Research Laboratories, Santa Barbara, California, as part of an overall research program on meteoroid protection concepts and design data for space radiators (NASA Contract nos. - NASw-468 and NAS3-2798). Prior results from the same program were reported in reference 7.

The report includes a description of the targets and their fabrication processes together with the test results and associated observations. The data obtained were principally qualitative in nature and therefore are presented in the form of photographs. Measurements of the target damage were made and are presented together with the crater depth correlation and analysis of the damage patterns.

APPARATUS

Ballistics Range Facility

All tests were performed on a ballistic range similar to the facility described in

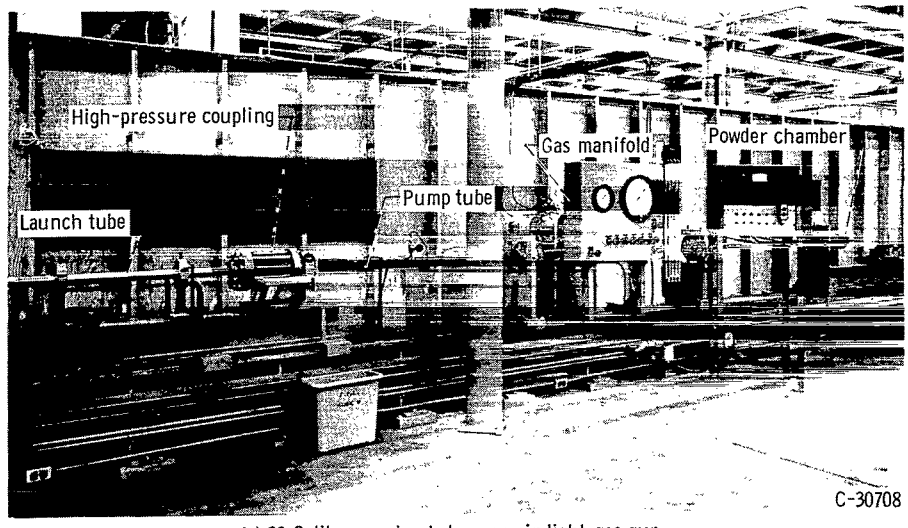

(a) 30 Caliber accelerated-reservoir light-gas gun.

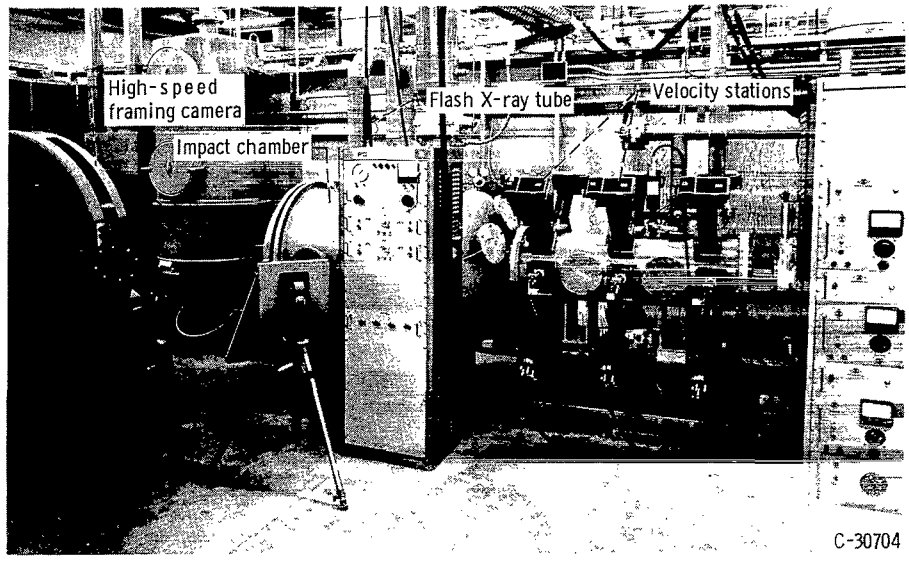

(b) Velocity measuring stations and impact chamber.

Figure 2. - Ballistics range facility at General Motors Corporation Defense Research Laboratory, Santa Barbara, California.

reference 8. The basic equipment consists of a light-gas gun, a 20-foot free-flight range, and an impact chamber. A photograph of the 30-caliber accelerated-reservoir light-gas gun is shown in figure 2(a). This facility can achieve nominal velocities of about 25 000 feet per second for routine testing; consequently, 25 000 feet per second was chosen as the nominal impact velocity for this investigation.

The accelerated-reservoir light-gas gun consists of a powder chamber in which smokeless powder is used to accelerate a polyethylene pump piston down an 18-foot-long, 1-inch-inside-diameter pump tube. In so doing, the piston compresses hydrogen as the driver gas to a nominal pressure of 20 000 to 30 000 pounds per square inch. At this

pressure, a break valve opens at the front end of the high-pressure coupling, thus releasing the hydrogen gas into the launch tube behind the projectile and sabot. As the projectile and sabot begin their travel in the 6-foot-long launch tube, the pump piston enters the tapered section of the high-pressure coupling. The front face of the pump piston is accelerated, thus maintaining a constant base pressure behind the saboted projectile during launch. The projectile is launched into the flight range and travels approximately 20 feet before impacting the target. Prior to impact, the saboted projectile travels through a surge chamber (not shown) in which the sabot is removed, allowing the projectile to continue into the velocity chamber (fig. 2(b)). Here, the position and time of arrival of the projectile are recorded at each of three shadowgraph stations. When the projectile interrupts a photobeam, electronic counters are stopped, and a short duration spark is set off at each section, exposing a film plate. The measurements of time and distance between stations serve to determine the velocity of the projectile along its trajectory and at the target. The accuracy of the impact velocity determined in this manner is ±1 percent.

The flight of the projectile is terminated in a specially constructed impact chamber that has several viewing ports (fig. 2(b)). A full-size door, which acts as the rear wall of the chamber, allows easy insertion and removal of the targets. The targets are held by a mounting supported on two rails on the floor of the chamber. This design allows the placement of the target at a uniform longitudinal position with respect to the viewing ports. A variety of targets can be accommodated.

Since the investigation of the damage to a radiator target requires that the target be impacted while under a simulated space environment, the tests were conducted with the target at an elevated temperature and at low ambient pressure. Special target mountings and heaters (fig. 3) permitted routine testing at temperatures up to 1400° F and selected testing at 2000° F. Generally, target heating was accomplished by electric resistance elements conforming to the surface of the target or through the use of a specially constructed furnace (fig. 3) that contained the entire target. The target temperature was monitored continuously by several thermocouples affixed to the specimen, and the heat was applied gradually to minimize any internal thermal gradients (e.g., approximately 2 to 3 hr were allowed for a tubular target).

The requirement for low ambient pressure was approached by sealing the impact and velocity chambers and pumping down to a pressure of less than 1 millimeter of mercury. To prevent oxidation of the heated targets in these tests, helium was used as the environmental gas in the impact chamber. A vacuum gage, calibrated for helium gas, provided an accurate measurement of the pressure within the chamber.

In general, most beryllium compounds are considered toxic, and ingestion, inhalation, or contact with the skin is to be avoided (ref. 9). The chamber was therefore modified to permit the testing of beryllium metal targets under hypervelocity impact at

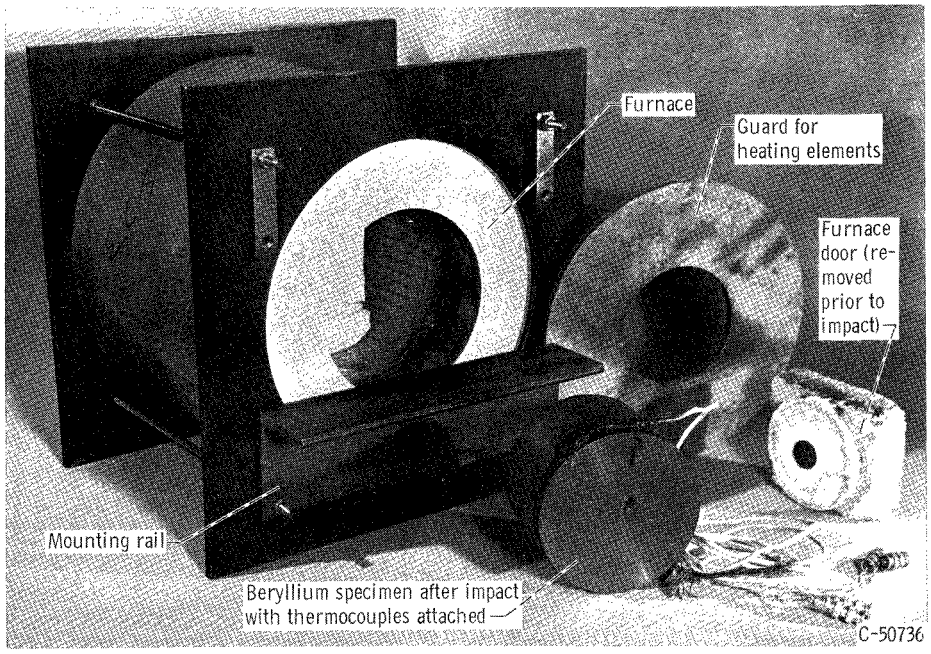

Figure 3. - Furnace used to heat plate and disk impact targets.

elevated temperature. A scavenging system was added to provide sufficient air purging or water flushing after impact to remove the particulate beryllium to the limiting maximum allowable concentration of 2 micrograms of beryllium per cubic meter (ref. 9). After safe conditions were attained and the targets were cool, they were thoroughly rinsed in water, dried, and placed in individual transparent bags for subsequent handling, examination, and storage.

Targets

The targets were selected to investigate impact effects into configurations ranging from semi-infinite flat plate targets to impacts into armored radiator tubes with inner liners. Large diameter flat plates of thicknesses up to 4 inches were used to obtain an assessment of the minimum impact damage characteristics of each material while small armored tubes (e.g., 0.50-in. i.d.) were used to assess the damage that might occur in space radiator tubes.

The beryllium targets were procured as finished targets that covered a range of processing methods and degrees of purity. The flat targets, fabricated from commercial grade, hot-pressed beryllium, were in the shape of thick circular disks having diameters of 4 or 6 inches with various thicknesses. The tubular targets consisted of beryllium armor 1.25-inch outside diameter by 0.375-inch wall thickness surrounding a 0.50-inch-outside-diameter tubular liner of AISI 316 stainless steel or columbium - 1-percent-

TABLE I. - BERYLLIUM TARGET DIMENSIONS AND COMPOSITION

Target number	Type	Liner tube			Armor				Brinell hardness number (a)
		Material	Inside diameter, in.	Wall thickness, in.	Outside diameter, in.	Thickness, t, in.	Composition from table II, column-	Processing method	
1	Disk	None	-----	-----	6.0	4.000	F	Hot pressed	142
2	Disk	None	-----	-----	6.0	.500	F	Hot pressed	147
3	Disk	None	-----	-----	4.0	1.000	D	Hot pressed	137
4	Disk	None	-----	-----	4.0	1.000	E	Hot pressed	128
5	Tube	AISI 316 SS	0.460	0.020	1.250	.373	A	Sintered powder	140
6	Tube	AISI 316 SS	.445	.028	1.229	.365	B	Extruded	154
7	Tube	Cb-1Zr	.400	.050	1.260	.380	C	Cast	[b]85 to 114
8	Tube	AISI 316 SS	.460	.020	1.250	.373	A	Sintered powder	140
9	Tube	AISI 316 SS	.480	.010	1.250	.375	A	Sintered powder	154
10	Tube	AISI 316 SS	.480	.010	1.250	.375	A	Sintered powder	154

[a]Room temperature values, 500 kg load with 10 mm ball.

[b]Range of 5 readings, very nonhomogeneous material.

zirconium alloy. These liner materials are considered representative of the two general classes of materials that could be used in radiator construction. No attempt was made in this investigation to assess the relative merits of these liner materials for resistance to hypervelocity impact. The inner liner thickness ranged from 0.010 to 0.050 inch. The 0.375-inch armor thickness was selected to prevent perforation of the liner tube as determined from previous empirical impact relations. The tubular beryllium targets were fabricated by first cold-pressing beryllium powder around the tube liner and then bonding and sintering it by the simultaneous application of heat and pressure. Solid extruded beryllium tubing was bonded to the tube liners by the same process. Beryllium armor was also cast directly around columbium - 1-percent-zirconium-alloy tubes through the use of special processes and molds. Specific details of these fabrication processes are found in references 10 and 11. Construction specifications and dimensions for the beryllium targets tested in this investigation are included in table I. Brinell hardness measurements were made on all beryllium targets and these also appear in table I. The chemical composition and available strength data for each beryllium target tested are found in table II.

The graphite materials were generally obtained in bulk form from the manufacturer and the individual targets were fabricated to specific geometries (e.g., rectangular blocks, flat plates, and tubes). The grades of graphite tested were AGSR, ATJ, ZTA (ref. 12), and pyrolytic (ref. 13); thus both the structural and premium quality grades were covered. The dimensions of each target prior to impact are recorded in table III. A general description of the distinguishing features for each grade is included in table IV.

TABLE II. - BERYLLIUM CHEMICAL ANALYSIS AND MECHANICAL PROPERTIES

Column	A	B	C	D	E	F
Target number	5, 8, 9, 10	6	7	3	4	1, 2
Target fabrication reference	10	10	11	--	--	--
Material identification	Powder	Extruded	Cast	Hot pressed	Hot pressed	Hot pressed
Element[a]:						
Beryllium	99.5	98.51	99.7	98.28	99.12	98.6
Beryllium oxide	.58	1.61	.19	1.90	1.51	1.67
Boron	.00008	1.1 ppm	---	----	----	----
Silver	.005	5 ppm	5 ppm	----	650 ppm	----
Aluminum	.075	.075	440 ppm	400 ppm	.103	.08
Carbon	.07	.040	.038	.128	----	.13
Calcium	<.01	200 ppm	<200 ppm	----	----	---
Cadmium	<.00007	1 ppm	--------	----	----	---
Cobalt	.0005	5.3 ppm	<5 ppm	----	----	---
Chromium	.01	73 ppm	55 ppm	----	----	---
Copper	.009	73 ppm	65 ppm	----	----	---
Iron	.080	.149	570 ppm	1600 ppm	1350 ppm	.11
Lithium	.0001	.5 ppm	-------	--------	--------	---
Magnesium	.012	.005	40 ppm	50 ppm	70	.004
Manganese	.0125	.013	120 ppm	------	--	----
Molybdenum	<.002	10 ppm	<10 ppm	------	--	----
Nitrogen	.02	------	-------	------	--	----
Nickel	.014	.017	110 ppm	------	--	----
Lead	<.001	3 ppm	3 ppm	------	--	----
Silicon	.02	-----	380 ppm	350 ppm	450 ppm	.04
Titanium	[b]---	-----	230 ppm	-------	-------	---
Zinc	---	100 ppm	<100 ppm	-------	-------	---
Mechanical Properties:						
Specific gravity	---	-------	--------	-------	-------	1.85
Ultimate tensile strength	---	-------	--------			
Longitudinal, psi				51 250	45 800	46 400
Transverse, psi				-------	-------	49 000
Yield strength	---	-------	--------			
(0.2 percent offset)						
Longitudinal, psi				35 300	31 070	32 600
Transverse, psi				------	------	32 600
Elongation	---	-------	--------			
Longitudinal, percent				1.88	1.85	1.5
Transverse, percent				----	----	2.0

[a]Analysis shown in percent unless otherwise noted.

[b]Dashes denote values not reported.

TABLE III. - GRAPHITE TARGET DIMENSIONS AND COMPOSITION

Target number	Type	Armor				Liner material
		Material grade	Orientation between impact direction and grain	Planform dimension, in.	Thickness, in.	
11	Block	ATJ	Across	4.0 square	2.00	None
12	Block	ATJ	Across	3.5 square	2.00	↓
13	Block	ATJ	Across	4.0 square	2.00	
14	Block	ZTA	Across	4.0 square	2.50	
15	Block	Pyrolytic	Across	4.0 square	2.50	
16	Block	Pyrolytic	With	4.0 square	2.50	
17	Tube	AGSR	Across	2.50 o.d.	[a]1.00	

[a]Tube wall thickness.

TABLE IV. - SUMMARY OF GRAPHITE GRADES TESTED

Grade	Bulk specific gravity	General characteristics	Composition and property reference
AGSR	1.54 to 1.58	Structural quality, general purpose, coarse grain, extruded with minor internal voids, not pitch impregnated	12
ATJ	1.73	Premium quality, fine grain, flaw free, high strength	12
ZTA	1.95	Premium quality, high density, controlled grain orientation, anisotropic mechanical and thermal properties, no structural macroflaws	12
Pyrolytic	2.20 to 2.23	Premium quality, high degree of property anisotropy, approaches maximum theoretical specific gravity (i.e., 2.266)	13

TABLE V. - BERYLLIUM TEST RESULTS

Target number	Report figure number	Impact round number	Target temperature, °F	Projectile[d]				Impact angle, λ, deg	Crater depth, P_∞, in.	Dimple height inside liner tube, in.	Ratio of penetration depth to target thickness, P_∞/t	Crater diameter, in.	Modulus of elasticity, psi	Calculated materials coefficient, γ[e]	
				Diameter, in.	Material	Mass, g	Impact velocity, ft/sec							Exponent φ	
														1/2	2/3
1	4	D-944	1300	3/32	Pyrex	------	23 700	0	0.190	-----	0.0475	0.23	[a]26.0×10^6	2.14	2.05
2	5	D-1087	1300	3/32	↓	0.0182	23 800	0	.197	-----	.394	.22	[a]26.0	2.21	2.11
3	6	D-147	700	3/32		.0178	24 700	0	.185	-----	.185	.25	[a]42.0	2.38	2.27
4	7	D-414	1300	3/32		.0176	25 800	0	.219	-----	.219	.25	[a]26.0	2.33	2.21
5	8, 9	D-416	1300	3/32		.0174	[c]25 300	0	.207	0.109	.555	.25	[b]20.0	2.05	1.96
6	8	D-770	1350	3/32		.0178	24 000	8	.201	.164	.551	---	[a]24.8	2.21	2.11
7	8	D-940	1300	3/32		.0178	24 300	8	.260	.060	.684	---	[b]20.0	2.66	2.53
8	9	D-415	Room	3/32		.0176	25 650	0	.161	.082	.442	.17	[a]43.0	2.05	1.95
9	10	D-1093	1300	3/32		.0180	24 000	55	.162	.112	.432	.20	[b]20.0	2.41	2.30
10	10	D-1094	1300	3/32		.0177	24 000	55	.160	.088	.427	.24	[b]20.0	2.39	2.28
														av 2.28	av 2.18

[a]Reference 18, 2 percent beryllium oxide.

[b]Reference 18, 1 percent beryllium oxide.

[c]Estimated.

[d]Average calculated specific gravity, 2.51 for 3/32-in.-diam. pyrex spheres.

[e]Based on target specific gravity, 1.85.

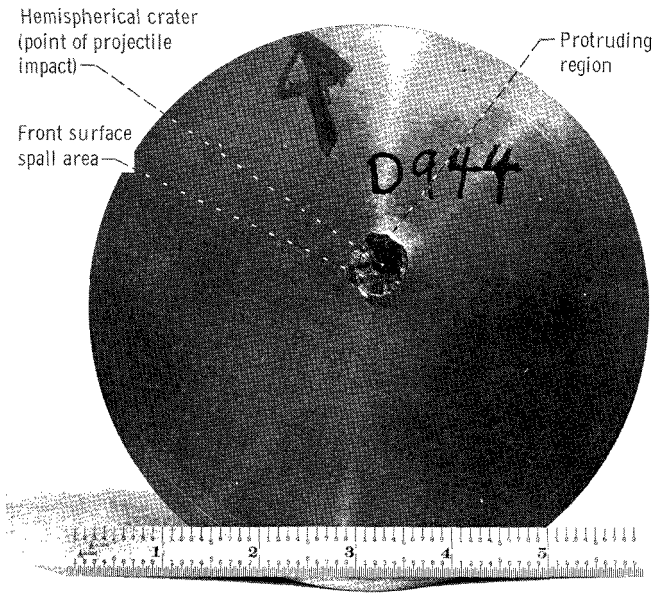

Figure 4. - Characteristic external primary damage in a semi-infinite beryllium target (target 1, 6-in. o. d. by 4-in. thickness). Impact velocity, 23 700 feet per second with 3/32-inch-diameter pyrex sphere; target temperature, 1300° F.

After hypervelocity impact testing, the pertinent external features of all targets were photographed and the crater depths were defined with respect to the original target surfaces. Crater diameters were also measured and recorded. For tubular targets, measurements of the dimple height dimension (protrusion of the inner surface of the tube under the point of impact) inside the tube were also made and recorded. The angle between the impact direction and the normal to the surface was also measured and recorded.

BERYLLIUM TARGET RESULTS

Thick Disks

All of the disk targets were fabricated from commercial grade, hot-pressed beryllium material having a beryllium oxide content of less than 2 percent. The targets were tested under nominally the same velocity conditions (25 000 ft/sec) with 3/32-inch-diameter pyrex spheres. Thus the qualitative observations that follow should not reflect any significant variation due to the beryllium target chemical composition. The beryllium impact data are presented in table V.

The damage on a semi-infinite beryllium target (fig. 4) was attained by impacting a 6-inch-diameter by 4-inch-thick disk. The target was heated to 1300° F and then impacted by a 3/32-inch-diameter pyrex sphere at a velocity of 23 700 feet per second. The front surface spalled region surrounding the hemispherical crater is typical of impact craters in brittle materials. The areas damaged by impact in such materials as lucite, glass, and rock have a similar appearance (refs. 5, 14, 15, and 16). In rock targets the origin of the front surface spall has been traced to internal failure along the trajectories of maximum shear (ref. 14). It is conjectured that the front spall fractures in beryllium are similarly governed since the protruding region surrounding the spall area shown in figure 4 suggests damage originating beneath the target surface. The rear surface of this beryllium target had no observable deformation or damage.

Reducing the target thickness to 0.50 inch and maintaining the same nominal impact conditions resulted in additional damage features not present in the semi-infinite target as shown in figure 5. The characteristic brittle primary damage (crater and spalled area) on the front surface of the target is seen; however, a portion of the front surface spalled material remained partly attached to the target. This observation serves to confirm that the front spall fracture originates beneath the surface and that the spalled material is removed as fragments. Several strong random fractures can also be seen on the front surface of the target; however, their random direction indicates no obvious

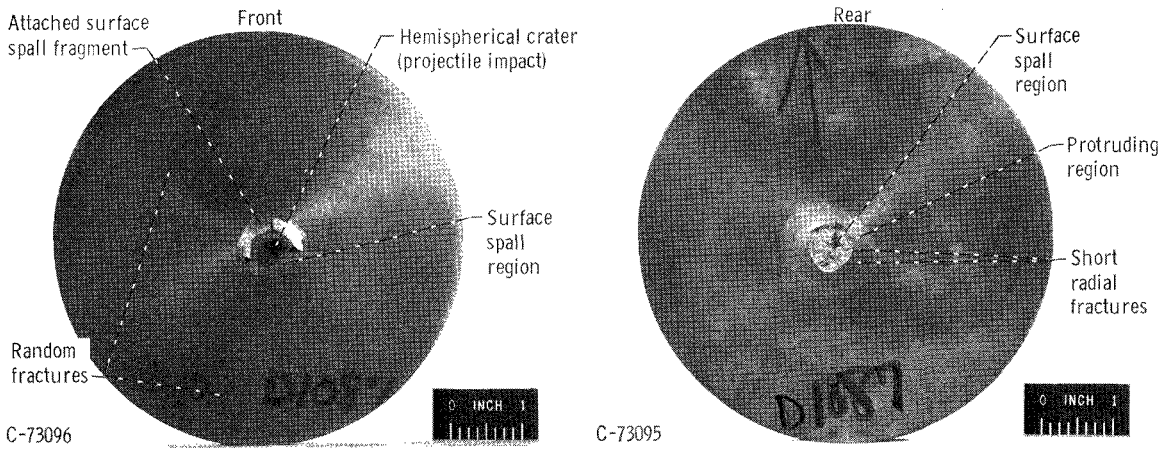

Figure 5. - Surface spall characteristics of a 6.0-inch-diameter by 0.50-inch-thick beryllium disk target (target 2). Impact velocity, 23 800 feet per second with 3/32-inch-diameter pyrex sphere; target temperature, 1300° F.

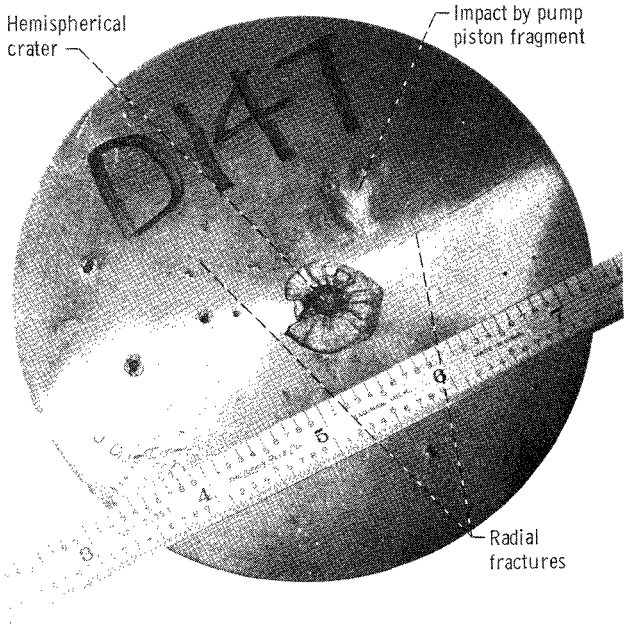

Figure 6. - Impact into a 4.0-inch-outside-diameter by 1.0-inch-thick hot-pressed beryllium disk (target 3) at 700° F. Impact velocity, 24 700 feet per second with 3/32-inch-diameter pyrex sphere.

direct relation to the cratering process and suggests that they may represent an extension of defects in the target.

The rear target surface (fig. 5) showed spall damage and also exhibited several distinguishing characteristics. The exposed surface left by the detached spall is sharply outlined and relatively flat. The protruding portion around the spalled area together with the short radial fractures suggests additional internal damage. Random fractures observed on the front surface were not visible on the rear surface of the target.

Targets with a 4.0-inch diameter and a 1.0-inch thickness were impacted at 700° and 1300° F to assess the effects of a reduction in target planform area and a variation in target temperature. Figure 6 depicts the results of the 700° F test temperature and reveals primary front surface damage consistent with the previous tests. Two radial fractures are visible on the front surface, one of which is strongest at the edge of the specimen. This fracture could have been initiated by the interaction of stress waves and the target boundary. This particular target, however, was inadvertently subjected to an additional impact by the plastic pump piston from the light-gas gun. The impact location of this fragment is shown on the figure and is a smooth, shallow depression. Debris of this nature generally travel at velocities of approximately 2000 feet per second and possess sufficient energy to extend and increase the damage caused by the projectile or to initiate new target damage.

The rear surface of the target (not shown) was not spalled by the impact of the projectile; however, several fine fractures were observed radiating from a point directly beneath the point of impact.

A companion target having the same dimensions as target 3 (fig. 6) and made from the same material was then impacted at 1300° F. Figure 7 indicates that the primary crater area had the same general features as that in the previous targets; however,

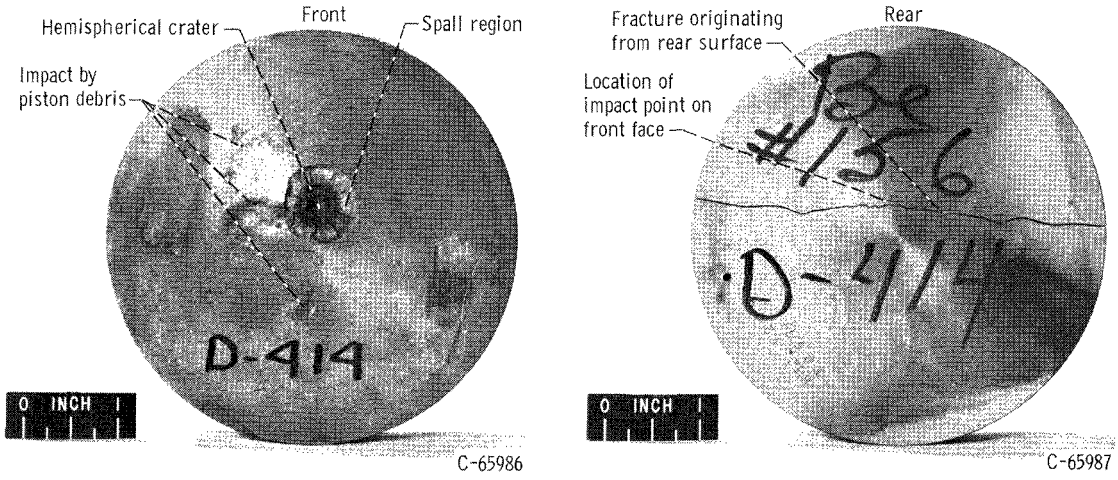

Figure 7. - Impact into a 4.0-inch-outside-diameter by 1.0-inch-thick hot-pressed beryllium disk (target 4) at 1300° F. Impact velocity, 25 800 feet per second with 3/32-inch-diameter pyrex sphere.

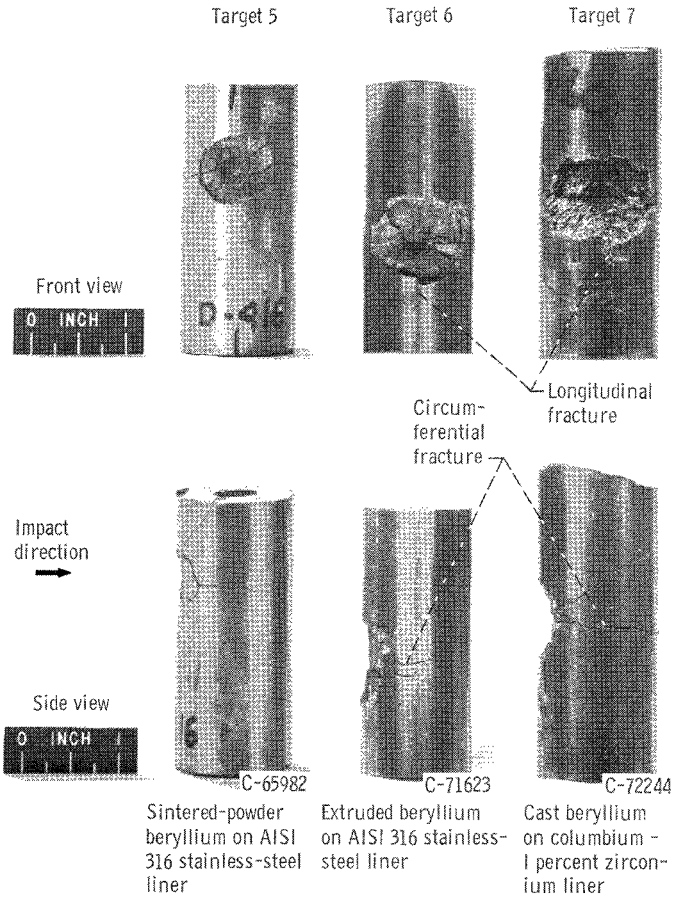

Figure 8. - Results of impact into beryllium - armored tubes fabricated by different processing methods. Impact velocity, 25 000 feet per second (nominal) with 3/32-inch-diameter pyrex sphere; target temperature, 1300° F.

there were no front radial fractures observed on this particular specimen. This phenomenon could be attributed to an apparent increase in ductility at the higher test temperature, since at high strain rates a trend toward increased ductility at temperatures around 1300° F has been displayed by commercial grade hot-pressed beryllium in conventional tensile tests (ref. 17).

This target was also subjected to additional impacts by pump piston debris, and the strong jagged fracture that appears in the rear view of figure 7 is presumed to be caused by the impact of these debris. No rear surface spall was visible on this target as was visible for the 700° F test shown in figure 6.

Tubes

Processing method. - Figure 8 illustrates the external impact damage on targets fabricated by different processing methods. The targets shown were fabricated from sintered-powder, extruded, or cast beryllium. All of the targets shown in figure 8 were impacted at a nominal temperature of 1300° F.

All the tubular targets showed essentially the same general damage patterns. In all cases a hemispherical crater was present surrounded by a spalled region, however, each of the processing methods had a somewhat different effect on the extent and appearance of the external damage. The front spalled region of the sintered-powder beryllium armored target covered the smallest area while the front spalled region on the extruded beryllium armored target covered approximately a 35 percent greater area. Both targets had the same texture on the spall fracture surfaces. The cast beryllium armored target had a 90-percent increase in front surface spalled area compared with the sintered-powder beryllium armored target. Also, the spall fracture surfaces of the cast target was noticeably more coarse and uneven as compared with those of the other two targets. It is surmised that this difference in fracture surface appearance is

attributable to the larger grain size encountered in cast beryllium.

The beryllium armor fabrication process also had an influence on the intensity of the cracks that occurred in several preferred orientations to the tube axis. All the beryllium targets shown in figure 8 had a strong circumferential crack radiating from the impact point that propagated around each target in a plane normal to the longitudinal axis of the tube. This crack was least severe in extent for the sintered-powder beryllium armor and most severe in extent for the cast beryllium armor. There was also a tendency for strong longitudinal cracks to develop on the front surfaces of both the extruded and cast armor as indicated in figure 8. This crack extended the entire length of the target and, by observing the end of the target, extended completely through the armor thickness. The longitudinal cracking is consistent with the directional properties induced in the extruded beryllium and the grain orientation in the tubular beryllium castings (ref. 11). Several longitudinal fractures were also observed on the rear external tube surface approximately opposite the impact point on all the targets.

The damage to the inner surface of the liner tubes for all the targets shown in figure 8 was confined to a hemispherical protrusion or dimple inside the tube bore. Visual examination did not reveal any observable cracks or openings in the liner tube. Measurements taken of the dimple height appear in table V (p. 10).

The cracks radiating from the impact point and extending beyond the front spall region were not observed on the beryllium disk targets described in the section entitled Thick Disks. The radial cracking pattern is believed to be a characteristic of brittle tubular targets and similar patterns have been observed on tubular lucite targets (ref. 5).

Temperature level. - The effect of target temperature on the results of impact into sintered-powder beryllium armored tubular targets is illustrated in figure 9. The tubular targets were tested at room temperature and 1300° F. Both targets revealed the characteristic hemispherical depression at the point of projectile impact. The same pattern of cracks radiating from the point of impact appeared on both the targets shown in figure 9. The principal observable difference between the two targets was that the front surface spalled region surrounding the point of impact in the target tested at room temperature covered approximately a 35 percent larger area and had a more irregular texture than the front surface spall of the target tested at 1300° F. A possible explanation for the larger front surface spall area could be the low room-temperature values of tensile elongation of beryllium (ref. 18) and the increased sensitivity of beryllium at room temperature to surface flaws induced by machining (ref. 17). No large differences in the dimples of the inner liner were observed, and there were no strong longitudinal cracks on the front surfaces of either of the targets. Each target, however, had similar longitudinal cracks on the rear external surface approximately opposite the impact point. The tests did not reveal any other major variations in the behavior of the beryllium armor attributable to the change in test temperature.

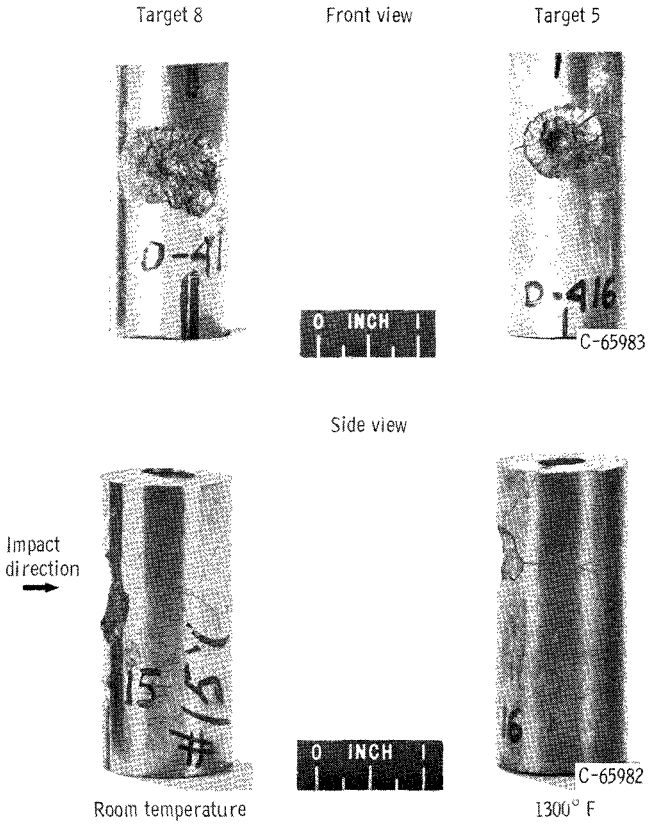

Figure 9. - Effect of target temperature on sintered-powder beryllium armor applied over 0.50-inch-outside-diameter by 0.028-inch-wall AISI 316 stainless-steel tubing. Impact velocity, 25 000 feet per second (nominal) with 3/32-inch-diameter pyrex sphere.

Multiple impacts. - The accidental impacts of gun debris on flat beryllium disks resulted in additional damage to the targets shown in figures 6 and 7 (pp. 12 and 13). If multiple meteoroid impacts occurred in service on beryllium armored tubes, the damage might likewise be magnified. Meteoroid impacts in close proximity on radiator tubes could aggravate or increase fractures already present from the previous impacts and possibly result in the separation or removal of large pieces of the armor from the liner tube. Consequently, if large amounts of beryllium armor material are lost, the reliability of the entire radiator structure could be substantially reduced.

A rather severe service impact condition was simulated by subjecting a sintered-powder beryllium armored tube to two impacts approximately 120° apart under the same test conditions. The results are shown in figure 10. A connecting fracture was observed between the two impact points, but no local separation or loss of armor occurred. Neither of the impacts perforated the interior stainless-steel tube, and no large differences in dimple height were obtained.

In service, the probability of the occurrence of high-energy meteoroid impacts in the same location is quite low. Lower energy impacts by smaller meteoroids are more likely to occur in close proximity; however, it is felt that the effects of these lower energy impacts would be comparatively weak and would not significantly contribute to the local damage.

GRAPHITE TARGET RESULTS

The impact data for the graphite targets tested in this phase of the investigation are listed in table VI. The graphite targets were generally in the form of thick rectangular solids; however, one tubular graphite target was included in this series of experiments.

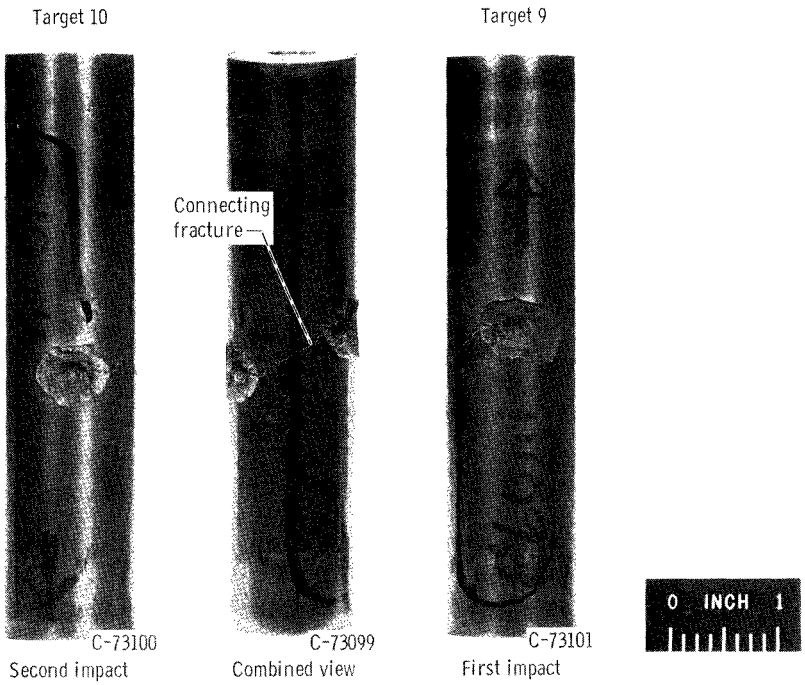

Figure 10. - Multiple impact on sintered-powder beryllium armored AISI 316-stainless-steel tube. Impact velocity, 24 000 feet per second (each impact) with 3/32-inch-diameter pyrex sphere; target temperature, 1300° F; angle between impacts, ~120°.

TABLE VI. - GRAPHITE TEST RESULTS

Target number	Report figure number	Impact round number	Target temperature, °F	Projectile[a]				Impact angle, λ, deg	Crater depth, P_∞, in.	Ratio of penetration depth to target thickness, P_∞/t	Crater diameter, in.	Modulus of elasticity, psi	Target specific gravity	Calculated materials coefficient, γ	
				Diameter, in.	Material	Mass, g	Impact velocity, ft/sec							Exponent φ	
														1/2	2/3
11	11	D-343	Room	1/8	Pyrex	0.0414	25 000	0	0.398	0.198	1.25	1.18×10^6 (ref. 22, p. 37)	1.73	1.16	1.08
12	11	D-362	1300	1/8	Pyrex	.0409	25 500	0	.406	.203	1.25	1.21 (ref. 22, p. 37)	1.73	1.18	1.11
13	12	D-371	Room	1/8	Aluminum	.0469	25 800	0	.414	.206	1.25	1.18 (ref. 22, p. 37)	1.73	1.09	1.01
														av 1.14	av 1.07
14	13	D-364	Room	1/8	Pyrex	.0412	25 400	0	.524	.210	1.69	.74 (ref. 22, p. 54)	1.94	1.32	1.27
15	14	D-361	1300	1/8	Pyrex	.0415	25 300	0	----	----	----	--- ----------	----	----	----
16	15	D-363	1300	1/8	Pyrex	.0413	25 600	0	.484	.194	1.50	4.4 (ref. 12)	2.20	2.41	2.19
17	16	D-991	1300	3/32	Pyrex	.0178	24 600	10	.359	.359	----	.90 (ref. 11)	1.57	1.27	1.17

[a]Average calculated specific gravity, 2.51 for 3/32-in.-diam. pyrex sphere; 2.47 for 1/8-in.-diam. pyrex sphere; and 2.80 for 1/8-in.-diam. aluminum sphere.

Blocks

The tests on graphite blocks used 1/8-inch-diameter pyrex spheres accelerated to the same nominal velocity of 25 000 feet per second as the 3/32-diameter pyrex spheres used in the beryllium tests discussed previously. Consequently the projectile energy at impact for the graphite tests was approximately 2.4 times that for the beryllium tests.

ATJ graphite. - The first experiments conducted on ATJ grade graphite were on 3.5- and 4.0-inch-square by 2.0-inch-thick blocks. The tests were conducted to ascer-

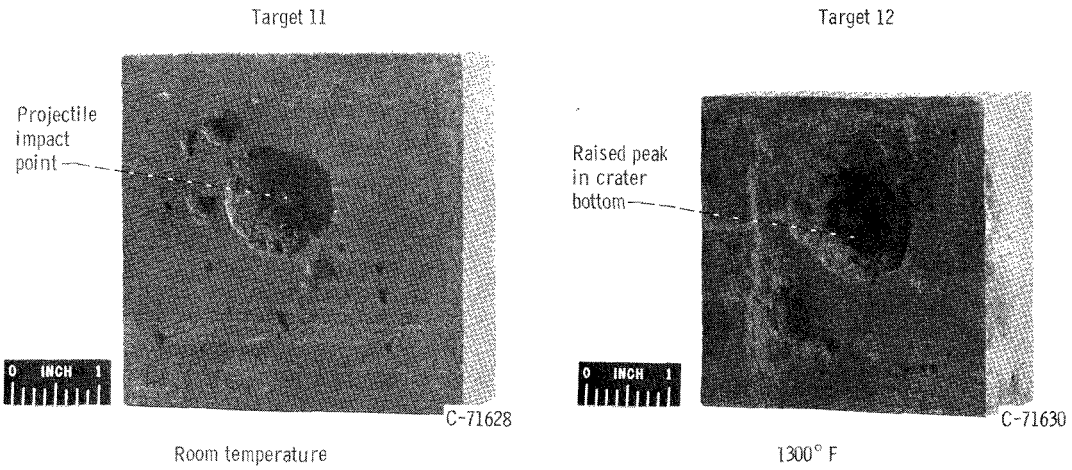

Figure 11. - Effect of target temperature on crater appearance in semi-infinite ATJ graphite block targets. Impact velocity, 25 000 feet per second (nominal) with 1/8-inch-diameter pyrex sphere.

tain the target damage of semi-infinite thick material at room temperature and at 1300^{O} F. The results are shown in figure 11.

The craters obtained were continuous, shallow, rough, and uneven. The small smooth hemispherical crater previously observed in the beryllium targets under the point of projectile impact was not present in the graphite target. The target tested at 1300^{O} F had a raised central portion or peak in the bottom of the crater as indicated in figure 11. The semi-infinite condition was attained as indicated by the absence of observable damage on the rear surface of the targets.

Even though 1/8-inch-diameter pyrex projectiles were used the greater energy did not cause any radial cracks to appear in the graphite targets. In this respect the behavior of the graphite in figure 11 was similar to the impact behavior of the flat semi-infinite beryllium target shown in figure 4. The supplementary small craters visible on the faces of the targets in figure 11 were presumed to be caused by miscellaneous gun debris. The increase in test temperatures from room temperature to 1300^{O} F had no observable effect on the appearance and size of the primary craters shown in figure 11.

The result of impact of a 1/8-inch-diameter aluminum projectile on an ATJ graphite target is shown in figure 12. The crater resulting from the aluminum projectile showed essentially the same features displayed by the craters caused by the pyrex projectiles. There was no visible damage on the rear surface of the target. Unfortunately, this target was inadvertently impacted by sizable fragments of debris (pump piston and/or sabot), and the close proximity of the debris to the projectile impact point resulted in additional crater and cracking damage as shown in figure 12. There was no visible damage on the rear surface of the target.

The impact crater had the same texture and shape as those shown in the targets of figure 11; however, there were several cracks radiating from the impact point to the adjacent edges. The projectile as well as the gun debris impacted this target quite close

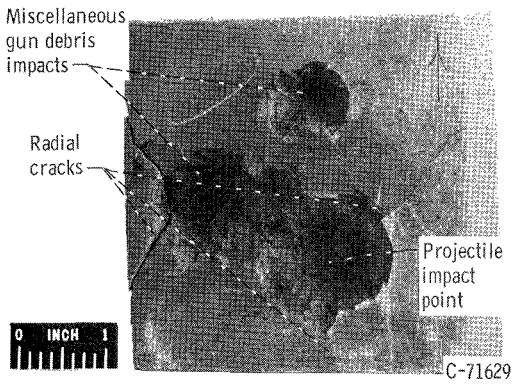

Figure 12. - Multiple impact of ATJ graphite block target (target 13, 4.0 in. square by 2.0 in. thick) at room temperature. Impact velocity, 25 800 feet per second with 1/8-inch-diameter aluminum sphere.

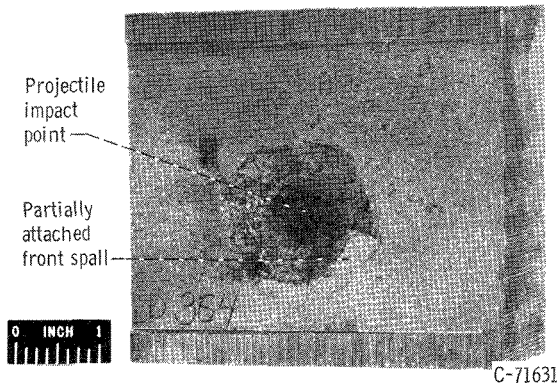

Figure 13. - Impact crater in ZTA graphite (target 14, 4.0 in. square by 2.5 in. thick). Impact velocity, 25 400 feet per second with 1/8-inch-diameter pyrex sphere at room temperature.

to the edges, and it is conjectured that this condition of proximity to the edges acted as an effective reduction in target size. Tensile waves reflected from the edges of the target are more likely to cause fractures as the target size is reduced. Similar effects attributable to a reduced target size have been observed in tests conducted with lucite and glass targets (ref. 5).

ZTA graphite. - Figure 13 illustrates the results of impact into ZTA graphite at room temperature. This grade of graphite represents an increase in density of 18 percent over the ATJ grade tested previously (see table IV, p. 9). In addition, anisotropic physical and thermal properties, controlled grain orientation, increased flexural strength, and macroflaw reduction are induced in this material by the manufacturing process (ref. 12). The crater shown in figure 13 was approximately conical in shape, in contrast to the craters observed in ATJ graphite (figs. 11 and 12). The impact crater also covered a larger diameter than did the craters in the ATJ targets. No radial fractures were observed around the impact point, nor was there visible damage on the target rear surface. A partly attached front spall was observed on this target as indicated in figure 13.

The texture of the material inside the crater had subtle differences compared with the material in the ATJ craters. The ZTA material had the appearance of "layers" or "flakes" normal to the direction of impact, which was presumed to be an effect of the material anisotropy.

Pyrolytic graphite. - The next series of experiments used pyrolytic graphite targets. This grade of graphite is made by deposition of carbon from a hydrocarbon gas on a heated graphite substrate (ref. 13). The material is deposited as a layered structure with a high degree of anisotropy. The plane of deposition is designated the a-b plane, and the thermal and physical properties parallel to the plane of deposition are on the order of 200 times greater than corresponding properties normal to the plane. The targets were 4.0 inches square by 2.5 inches thick and were composed of individual 1/4-

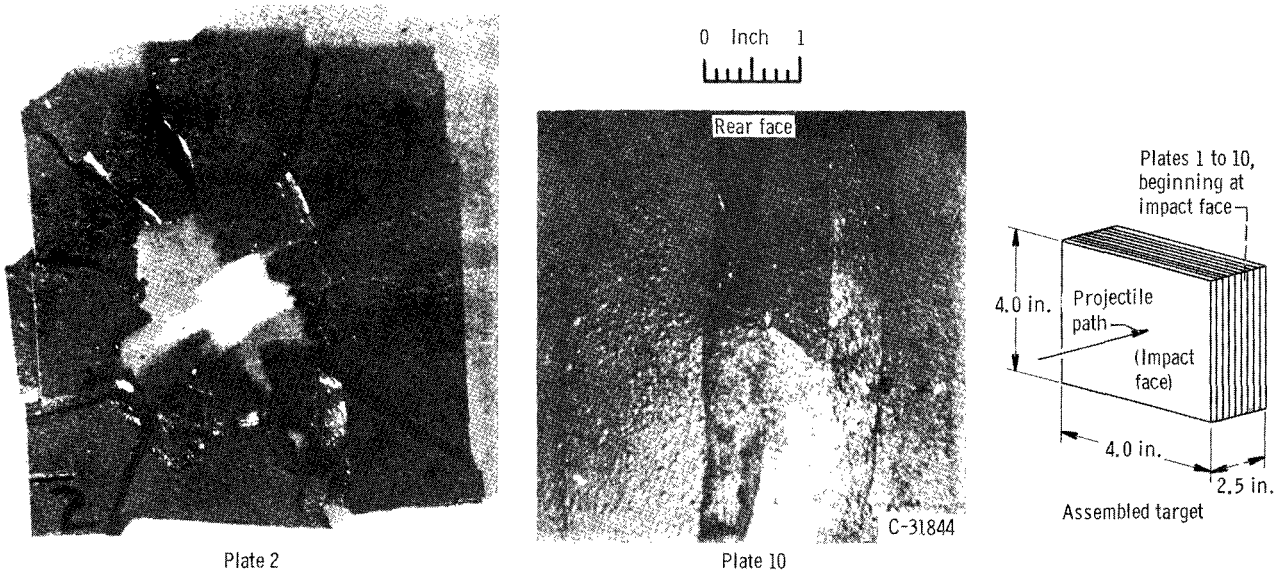

Figure 14. - Pyrolytic graphite semi-infinte target (target 15) with 10 individual plates (each 0.25 in. thick) oriented perpendicular to impact. Impact velocity, 25 300 feet per second with 1/8-inch-diameter pyrex sphere; target temperature, 1300° F.

inch-thick plates clamped together because usable thick plates could not be obtained. In the test, the plates were impacted on the 4.0-inch-square face. Two targets were assembled: one having the plates parallel to the impact direction; and the second having the plates normal to the impact direction.

In the tests of the effect of impact normal to the plates, each plate of the target was numbered consecutively beginning with the impact face as shown in figure 14. The first two plates were both perforated and suffered severe cracking and extensive fragmentation. Plate 3 suffered slight damage while plates 4 to 7 remained intact. The last three plates on the rear of the target were each damaged in a fashion suggesting rear spalling. Plates number 2 and 10 are shown in figure 14 to illustrate the nature of the damge in the two affected regions. Similar impact results for unbonded, laminated metal targets are indicated in reference 19. Reference 5 also cited additional damage occurring in thin brittle targets backed with heavier layers of other materials. The severe damage suffered by the first two pyrolytic graphite plates is thus conjectured to be a characteristic of the laminated unbonded construction of the target and not necessarily due to the anisotropy of the properties of the individual plates.

Figure 15 illustrates the results of impact into a clamped pyrolytic graphite target with individual plates oriented parallel to the impact direction. Each plate was numbered consecutively beginning at the left edge of the target as shown in figure 15. The observed crater covered a firmly outlined circular area, shallow in depth and rough and uneven in appearance. The damage sustained by this target had different characteristics from the target shown in figure 14 with the plates oriented perpendicular to the impact direction. None of the plates suffered the complete fragmentation observed on the previous target

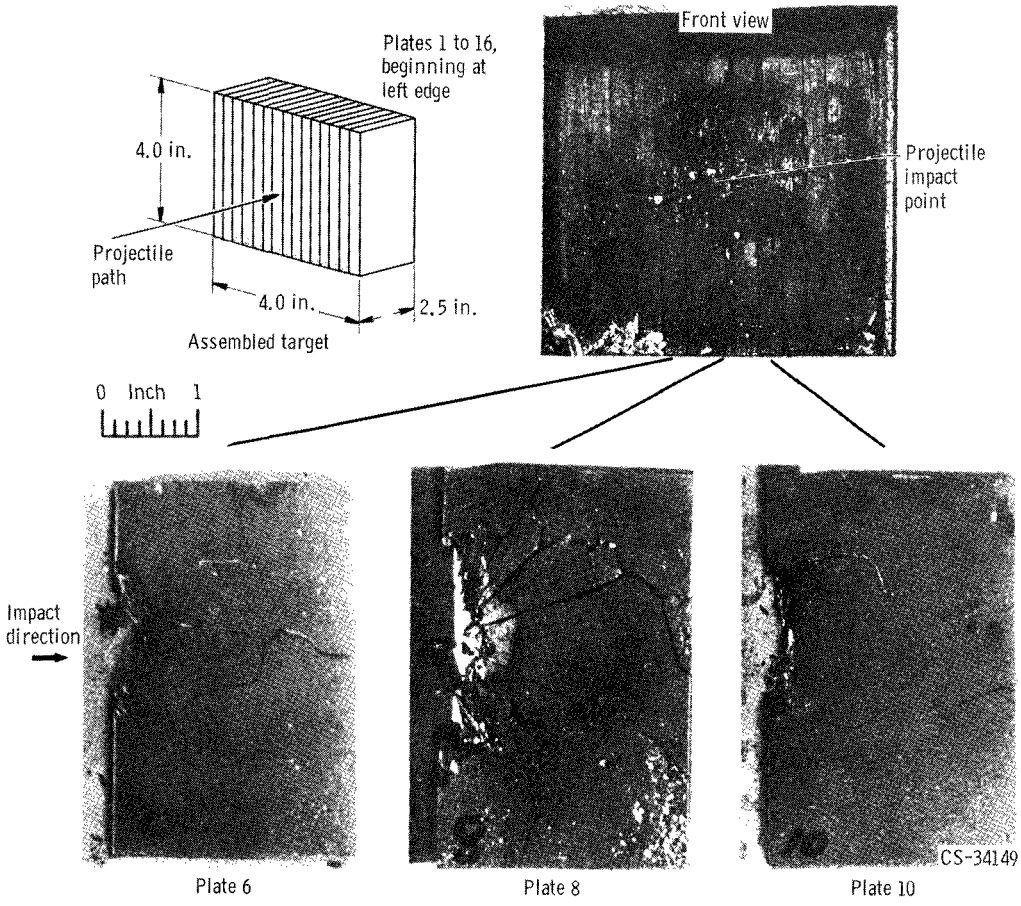

Figure 15. - Pyrolytic graphite semi-infinite block target (target 16) with individual plates oriented parallel to impact direction. Impact velocity, 25 600 feet per second with 1/8-inch-diameter pyrex sphere; target temperature, 1300° F.

since each damaged plate was partially restrained by the adjacent plates on either side. There was no rear surface spall damage such as seen on the previous target. Several plates near the projectile impact point, however, had cracks radiating from the point of impact to the rear surface of the target. Plate number 8 was located under the point of projectile impact and suffered the greatest damage. The damage decreased on plates to either side of the impact point. Figure 15 shows individual views of plates 6, 8, and 10 as representative examples of the trend of damage relative to the point of impact. The plates were held in position by clamps and were not bonded together; hence the damage just described is again influenced by the unbonded laminations. The comparisons of figures 14 and 15 indicate, however, that less overall target damage is encountered when the individual plates are oriented parallel to the direction of impact. The parallel orientation (fig. 15) is also the most probable armor configuration for space radiators since the maximum value of thermal conductivity occurs in the plane of the sheet.

Tubes

A cylindrical graphite target was fabricated from AGSR grade material having a 2.5-inch outside diameter by 0.50-inch bore. The AGSR grade was selected as being representative of the structural quality graphite material that might be suitable for space radiator armor. The results of impact into this target are shown in figure 16. The crater was similar in shape and texture to the craters observed in the ATJ graphite block targets (figs. 11 and 12). The inner surface of the bore was not damaged under the point of impact. Hence the results can be considered representative of an impact on a semi-infinite target. There was no evidence of the radial fracturing emanating from the crater or any other cracking such as found on the beryllium armored tubes. It is not certain whether the lack of cracking can be attributed to the increased wall thickness of the graphite tube or to the graphite material itself; however, it is noted that there was less tendency for radial cracking to occur in the graphite blocks than in the beryllium blocks.

ANALYSIS AND DISCUSSION

Penetration Relation

The initial comparison of the various candidate armor materials for waste heat radiators (ref. 3) was based on the following correlation obtained for hemispherical craters or penetration depths in semi-infinite flat plates:

$$\frac{P_\infty}{d} = \frac{\gamma}{4.21}\left(\frac{\rho_p}{\rho_t}\right)^{\varphi} \frac{(v \cos \lambda)^{2/3}}{\left(\frac{E_t}{\rho_t}\right)^{1/3}} \tag{1}$$

where

P_∞ penetration depth in a semi-infinite plate (crater depth), in.

d nominal projectile diameter, in.

γ target material correlating coefficient

ρ_p projectile specific gravity (calculated from the actual mass and nominal projectile diameter)

ρ_t target specific gravity

φ exponent (taken as 1/2 or 2/3)

v projectile velocity, ft/sec

λ angle of impact (for normal impact, $\cos \lambda = 1$)

E_t target modulus of elasticity, psi

Metallic materials generally exhibit γ values ranging from 1.5 to 2.5 (ref. 5); however a value of 2.0 was used for γ in the calculations of radiator weight made in reference 3 for all materials because of the lack of specific values for each material. Experimental values of P_∞ in conjunction with equation (1) were used to obtain values of γ for both the beryllium and graphite flat plate and tubular targets. The pertinent experimental and property data for beryllium and graphite targets are listed in tables V and VI (pp. 10 and 17, respectively) together with experimentally determined values of the materials coefficient γ for two values of the exponent φ. The targets listed in tables V and VI were considered essentially semi-infinite in thickness since the computed values of the ratio of crater depth to target thickness (P_∞/t) fell below the value of 0.75 arbitrarily set for thin targets in reference 5.

Table VII summarizes the calculated average values of materials coefficient for ex-

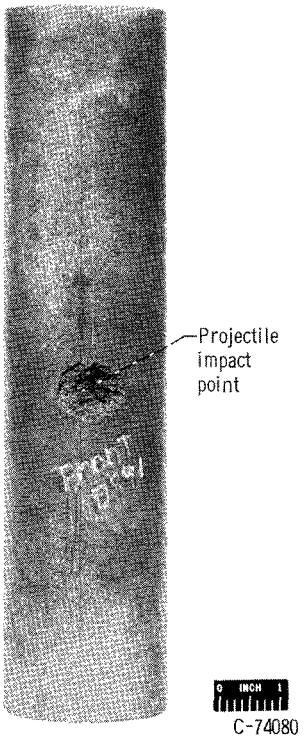

Figure 16. - AGSR graphite tube target (target 17, 2.50-in. o.d. by 0.50-in. i.d. by 12.0-in. length). Impact velocity, 24 600 feet per second with 3/32-inch-diameter pyrex sphere; target temperature, 1300° F.

TABLE VII. - SUMMARY OF CALCULATED MATERIAL COEFFICIENT

Material and Impact Orientation	Materials coefficient, γ		Number of tests
	Exponent φ		
	1/2	2/3	
Beryllium (disks and tubes)	2.28	2.18	10
ATJ Graphite (across grain)	1.14	1.07	3
ZTA Graphite (across grain)	1.32	1.27	1
AGSR Graphite (across grain)	1.27	1.17	1
Pyrolytic graphite (with grain)	2.41	2.19	1

ponent values of 1/2 and 2/3. The individual values of the materials coefficient for the beryllium data (10 values) and the graphite data (5 values) exhibited close agreement within each group of materials (tables V and VI).

The average γ values calculated for beryllium, 2.28 for $\varphi = 1/2$ and 2.18 for $\varphi = 2/3$, are in fair agreement for the values of φ published for other metals. These values are 1.96 for 1100 aluminum, zinc, tin, steel, cadmium, copper, and lead targets (ref. 20, $\varphi = 1/2$), 2.28 for lead and copper targets (ref. 21, $\varphi = 2/3$), and 2.27 for cast aluminum targets (ref. 5, $\varphi = 1/2$ and 2/3).

Generally, the manufacturing process for graphite induces a preferred grain orientation in all graphite products, which results in anisotropic mechanical and thermal properties (ref. 12). Consequently, the values of the modulus of elasticity used in computing the γ values for graphite were taken for the orientation of the grain parallel to the direction of impact (refs. 12, 13, and 22). The γ values calculated for the graphite targets impacted across the grain (i.e., ATJ, AGSR, and ZTA grades) consistently fell substantially below the experimental value for beryllium. Only the pyrolytic graphite specimen impacted with the grain showed a value of γ near the aluminum and beryllium values.

It is of interest to speculate about the possible reasons for the behavior of the graphite as revealed by the differences in the γ values. Equation (1) is an empirical description of the depth of penetration into fully dense ductile metals exhibiting hemispherical craters. The graphite craters were generally not hemispherical, which indicate perhaps that the interaction between the cratering process and the materials strength properties may be different in graphite. Also, all the graphite grades that were impacted across the grain exhibited shallower craters (lower γ) than those of the single target result impacted with the grain. This might suggest that material property anisotropy is strongly involved. Finally, recent investigations (e.g., ref. 23) have indicated that an increased ability to attenuate shock waves is possible with less than fully dense material. Thus, less penetration might be involved in the lower density grades (ATJ, ASGR, ZTA) than in the nearly maximum density pyrolytic grade. In any event, it is apparent that graphite crater depths may be considerably different from those of the more conventional metals under comparable impact conditions.

Application Considerations

If beryllium and graphite are considered as material for space radiator meteoroid protective armor, the preliminary data presented herein suggest several factors for consideration in the design application. The occurrence of cracking under hypervelocity impact for these materials indicates their unsuitability for carrying structural loads.

Furthermore, the existence of cracking damage in the beryllium disks and tubes suggests that significant cracking could also occur in thin beryllium and graphite fins, dependent on sheet thickness, size, and impacting particle energy (as was the case for thin lucite sheets in ref. 5). Consequently, additional investigations should be performed to evaluate the impact resistance of beryllium and graphite as thin fins for space radiators.

Although highly improbable, the combined effects of multiple impacts, vibration, creep, and thermal cycling could act on a cracked armor section and result in the local separation of the cracked material. Such local loss of armor would increase the vulnerability of the exposed inner liner to further impact damage. In addition it may be desirable to strengthen the armor to increase the structural capacity of the armor for load carrying purposes. Hence, it may be worthwhile to investigate concepts of reinforcing or containing the armor with metallic fibers or mesh.

Cracking can also result in a degradation of radiating effectiveness if the cracks occurred normal to the conduction heat flow path in the armor or at the junction of the armor and fin. Increased thermal degradation could also result in beryllium radiators because of the larger loss of high-emittance surface coating resulting from the increased spall area around the impact crater. This effect should not be as significant for graphite, however, because of its higher natural emittance (coatings may not be required, ref. 3). The significance of the preceding problems will depend on the ratio of damaged area to total radiator surface area that, in general, should be quite small.

Finally, further impact tests with thick graphite targets should be conducted to verify the low indicated value of the materials coefficient γ. If substantiated, a more favorable weight advantage for graphite might result; however, final comparisons will require the establishment of appropriate factors describing armor thickness required to prevent inner surface spall or other critical damage criteria in lined tubes.

SUMMARY OF RESULTS

The following are the major results of the study of damage characteristics of selected beryllium and graphite plate and tubular targets under hypervelocity impact conditions:

1. The impact craters in flat semi-infinite beryllium and graphite disk or block targets differed in appearance from impact craters in conventional ductile materials. Beryllium craters consisted of a relatively smooth hemispherical depression under the point of projectile impact surrounded by a larger sometimes irregular spalled region. Graphite craters generally consisted of a continuous, large, rough-textured, shallow crater. The appearance of these craters is not greatly affected by reductions in target planform area or increases in target temperatures up to 1300° F in block targets.

2. Beryllium and graphite tubular targets had craters similar in appearance to those

in comparable flat disk or block targets. Increasing the test temperature from room temperature to 1300° F in a beryllium sintered-powder tube target resulted in a sizable decrease in front spall area and a smoother texture of the spall fracture surface. Crater spall area was also observed to vary substantially for beryllium tubular targets made by different processing methods.

3. Cracking damage occurred on beryllium and some graphite flat disk or block targets and on beryllium tube targets. The cracks extended radially from the crater in most cases, and reductions in target planform area or multiple impacts tended to increase the severity of cracking damage. Strong longitudinal cracks were observed on the front surface in the beryllium tubular targets that were cast or extruded.

4. Multiple impacts of equal energy in the same vicinity on a sintered-powder beryllium armored tube did not result in any local removal or loss of cracked material.

5. The crater depths in beryllium plate and tube targets (10 samples) correlated according to the modulus of elasticity produced average materials coefficients of 2.18 to 2.28, similar to values experienced with other metallic materials. Crater depths in conventional graphite (ATJ, ZTA, AGSR), however, exhibited about 50 percent lower values based on the same correlation criterion. The variation of the individual values of the materials coefficient calculated for the beryllium data (10 values) and the graphite data (5 values) exhibited close agreement within each respective materials group.

Lewis Research Center,
National Aeronautics and Space Administration,
Cleveland, Ohio, June 28, 1965.

REFERENCES

1. Corliss, William R.: Survey of Space Power Requirements - 1962-1976. Progress in Astronautics and Aeronautics. Vol. 11 - Power Systems for Space Flight, M. A. Zipkin and R. N. Edwards, eds., Academic Press, 1963, pp. 3-13.

2. Krebs, Richard P.; Winch, David M.; and Lieblein, Seymour: Analysis of a Megawatt Level Direct Condenser-Radiator. Progress in Astronautics and Aeronautics. Vol. 11 - Power Systems for Space Flight, M. A. Zipkin and R. N. Edwards, eds., Academic Press, 1963, pp. 475-504.

3. Diedrich, James H.; and Lieblein, Seymour: Materials Problems Associated with the Design of Radiators for Space Powerplants. Progress in Astronautics and Aeronautics. Vol. 11 - Power Systems for Space Flight, M. A. Zipkin and R. N. Edwards, eds., Academic Press, 1963, pp. 627-653.

4. Rinehart, J. S.; and Pearson, J.: Behavior of Metals Under Impulsive Loads. ASM, 1954, ch. 9.

5. Diedrich, James H.: and Stepka, Francis S.: Investigation of Damage to Brittle Materials by Impact with High-Velocity Projectiles into Glass and Lucite. NASA TN D-2720, 1965.

6. Loeffler, I. J.; Lieblein, Seymour; and Clough, Nestor: Meteoroid Protection for Space Radiators. Progress in Astronautics and Aeronautics. Vol. 11 - Power Systems for Space Flight, M. A. Zipkin and R. N. Edwards, eds., Academic Press, 1963, pp. 551-579.

7. Lieblein, Seymour; Clough, Nestor; and McMillan, A. R.: Hypervelocity Impact Damage Characteristics in Armored Space Radiator Tubes. NASA TN D-2472, 1964.

8. Anon.: Research Facilities of the Aerospace Operations Department. Rept. No. ER 62-201A, Defense Res. Labs., General Motors Corp., 1962.

9. Sax, N. Irving: Dangerous Properties of Industrial Materials. Second ed., Reinhold Pub. Corp., 1963.

10. Diersing, R. J.; Hanes, H. D.; and Hodge, E. S.: Fabrication of Beryllium-Clad Tubular Hypervelocity Impact Targets by Gas Pressure Bonding. NASA CR-54058, 1963.

11. Patenaude, C. J.; and Santschi, W. H.: Casting of Beryllium - Stainless Steel and Beryllium - Columbium Impact Target Composites. NASA CR-54144, 1964.

12. Anon.: The Industrial Graphite Engineering Handbook. Second ed., Nat. Carbon Co., Union Carbide Corp., 1962.

13. Anon.: Pyrolytic Graphite Engineering Handbook. Special Alloys Div., General Electric Corp., July 15, 1963.

14. Maurer, W. C.; and Rinehart, J. S.: Impact Crater Formation in Rock. Proc. Fourth Hypervelocity Impact Symposium, Vol. III, (Rept. No. APGC TR-60-39), 1960.

15. Moore, H. J.; MacCormack, R. W.; and Gault, D. E.: Fluid Impact Craters and Hypervelocity - High-Velocity Impact Experiments in Metals and Rocks. Proc. Sixth Hypervelocity Impact Symposium, Vol. II, Pt. 2, 1963, pp. 367-399. (See also NASA CR-51340, 1963.)

16. Moore, H. J.; and Lugn, R. V.: Experimental Hypervelocity Impact Craters in Rock. Proc. Fifth Hypervelocity Impact Symposium, Vol. 1, Pt. II, 1961, pp. 625-643.

17. O'Rourke, R. G.; Hurd, J. N.; Wikle, K. G.; and Beaver, W. W.: Mechanical Properties of Reactor Grade Beryllium at Elevated Temperatures. Rept. No. COO-312, Brush Beryllium Co., Aug. 1956.

18. Beaver, W. W.; O'Rourke, R. G.; and Hurd, J. N.: Effect of Purity and Manufacturing Variables on Elevated Temperature Properties of Beryllium. STP No. 272, ASTM, 1960, pp. 81-94.

19. Gehring, J. W.; Christman, D. R.; and McMillan, A. R.: Hypervelocity Impact Studies Concerning the Meteoroid Hazard to Aerospace Materials and Structures. Proc. Fifth Annual AIAA Structures and Materials Conf., Palm Springs, Calif., Apr. 1-3, 1964, pp. 78-91.

20. Bruce, E. P.: Review and Analysis of High Velocity Impact Data. Proc. Fifth Hypervelocity Impact Symposium, Vol. I, Pt. II, 1961, pp. 439-474.

21. Summers, James L.: Investigation of High-Speed Impact: Regions of Impact and Impact at Oblique Angles. NASA TN D-94, 1959.

22. Dull, R. B.: Research and Development on Advanced Graphite Materials. Vol. XXVI - Physical Properties of Some Newly Developed Grades. Rept. No. WADD-61-72, May 1964.

23. Rae, W. J.: Nonsimilar Solutions for Impact-Generated Shock Propagation in Solids. NASA CR-54251, 1965, p. 74.

"The aeronautical and space activities of the United States shall be conducted so as to contribute . . . to the expansion of human knowledge of phenomena in the atmosphere and space. The Administration shall provide for the widest practicable and appropriate dissemination of information concerning its activities and the results thereof."

—NATIONAL AERONAUTICS AND SPACE ACT OF 1958

NASA SCIENTIFIC AND TECHNICAL PUBLICATIONS

TECHNICAL REPORTS: Scientific and technical information considered important, complete, and a lasting contribution to existing knowledge.

TECHNICAL NOTES: Information less broad in scope but nevertheless of importance as a contribution to existing knowledge.

TECHNICAL MEMORANDUMS: Information receiving limited distribution because of preliminary data, security classification, or other reasons.

CONTRACTOR REPORTS: Technical information generated in connection with a NASA contract or grant and released under NASA auspices.

TECHNICAL TRANSLATIONS: Information published in a foreign language considered to merit NASA distribution in English.

TECHNICAL REPRINTS: Information derived from NASA activities and initially published in the form of journal articles.

SPECIAL PUBLICATIONS: Information derived from or of value to NASA activities but not necessarily reporting the results of individual NASA-programmed scientific efforts. Publications include conference proceedings, monographs, data compilations, handbooks, sourcebooks, and special bibliographies.

Details on the availability of these publications may be obtained from:

SCIENTIFIC AND TECHNICAL INFORMATION DIVISION

NATIONAL AERONAUTICS AND SPACE ADMINISTRATION

Washington, D.C. 20546